

Optical Spectroscopy of the ULX-Associated Nebula MF16

Pavel ABOLMASOV^{1,2}, S. FABRIKA^{1,2}, O. SHOLUKHOVA¹

and

Taro KOTANI³

¹*Special Astrophysical Observatory, Nizhnij Arkhyz 369167, Russia*

²*University of Oulu, P.O. Box 3000, 90014, Finland*

³*Dept. of Physics, Tokyo Tech, 2-12-1 O-okayama, Tokyo 152-8551*

pasha@sao.ru, fabrika@sao.ru

(Received ; accepted)

Abstract

We present the results of optical panoramic and long-slit spectroscopy of the nebula MF16 associated with the Ultraluminous X-ray Source NGC6946 ULX-1. More than 20 new emission lines are identified in the spectra. Using characteristic line ratios we find the electron density $n_e \sim 600 \text{ cm}^{-3}$, electron temperature in the range from $\sim 9000 \text{ K}$ to $\sim 20000 \text{ K}$ (for different diagnostic lines) and the total emitting gas mass $M \sim 900 M_\odot$. We also estimate the interstellar extinction towards the nebula as $A_V \simeq 1^{\text{m}}.54$ somewhat higher than the Galactic absorption. Observed line luminosities and ratios appear to be inconsistent with excitation and ionization by shock waves so we propose the central object responsible for powering the nebula. We estimate the parameters of the ionizing source using photon number estimates and *Cloudy* modelling. Required EUV luminosity ($\sim 10^{40} \text{ erg s}^{-1}$) is high even if compared with the X-ray luminosity. We argue that independently of their physical nature ULXs are likely to be bright UV and EUV sources. It is shown that the UV flux expected in the *GALEX* spectral range (1000–3000 Å) is quite reachable for UV photometry. Measuring the luminosities and spectral slopes in the UV range may help to distinguish between the two most popular ULX models.

Key words: ISM: individual (MF16), jets and outflows, supernova remnants X-rays: individual (NGC 6946 ULX-1) ultraviolet: general

1. Introduction

1.1. ULXs and their Optical Nebulae

A point-like X-ray source in an external galaxy is considered an Ultraluminous X-ray source (ULX) if its luminosity exceeds 10^{39} erg s $^{-1}$ and it is not an active galactic nucleus. It also makes sense to exclude X-ray bright SNe and young (such as several years) Supernova Remnants (SNR) that can shine as bright as 10^{41} erg s $^{-1}$ in X-rays like the remnant of SN1988Z (Fabian & Terlevich 1996). There are more than 150 ULXs known at the present time (Swartz et al. 2004) but very little is clear yet about the physical nature of these objects.

ULXs are widely accepted as a class of accreting compact objects violating the Eddington luminosity limit for a conventional stellar mass black hole (about 1.3×10^{39} erg s $^{-1}$ for $10 M_{\odot}$). High luminosity may be a consequence of a higher accretor mass, supercritical accretion, mild geometrical collimation, relativistic beaming (Körding et al. 2002) or some combination of these effects. Two models are the most popular: (i) Intermediate-Mass Black Holes (IMBHs) with masses in the range $10^2 - 10^4 M_{\odot}$ (Colbert & Miller 2005; Madau & Rees 2001) accreting at sub-Eddington rates; (ii) supercritical accretion discs like that of SS433 around stellar mass black holes observed at low inclinations $i \lesssim 20^{\circ}$ (Katz 1986; King et al. 2001; Fabrika & Mescheryakov 2001). Some authors (Soria & Kuncic 2007) propose “hybrid” models involving $20 - 100 M_{\odot}$ black holes accreting in a moderately supercritical regime. Supercritical accretion discs are considered by different authors either in the wind-dominated regime first introduced by Shakura & Sunyaev (1973) or in the advection-dominated regime known as slim disc (Abramowicz et al. 1988; Okajima et al. 2007).

Large number of ULXs are surrounded by large-scale bubble nebulae (Pakull & Mirioni 2003), probably shock-powered. ULX nebulae (ULXNe), however, do not form a homogeneous class of objects. In Abolmasov et al. (2007) we review the observational properties of 8 ULXNe including the object under consideration. We conclude that only about 50% of ULXNe may be considered shock-powered shells. In some of the observed ULXNe high-excitation lines such as [O III] λ 4959,5007 are enhanced. In some cases HeII λ 4686 emission is detected as bright as 0.2–0.3 in H β units (Lehmann et al. 2005). The line may have stellar origin (Kuntz et al. 2005) as well as nebular. Measuring line widths may help to distinguish between these two cases. The nebulae may clarify the nature of corresponding X-ray sources in two ways: (i) probing the photoionizing radiation of the central object via gas excitation and ionization conditions; (ii) detecting and measuring jet/wind activity by kinematical effects and shock emission.

Dynamically disturbed gas may be considered an evidence against the IMBH hypothesis because a standard accretion disc is unlikely to produce strong jets or wind. Supercritical accretion, on the other hand, is supposed to provide a massive outflow in the form of a strong wind carrying practically all the accreted mass and having kinematical luminosity $\sim 10^{38}$ erg s $^{-1}$ in the case of SS433 (Fabrika 2004). Power comparable with the Eddington luminosity (\sim

10^{39} erg s^{-1}) may be provided in the form of relativistic jets. Their mechanical luminosity acting for $\sim 10^5$ years is sufficient to produce a wind-blown bubble with properties close to those of some of the existing ULX nebulae (Pakull & Mirioni 2003; Abolmasov et al. 2007).

ULXNe exhibit very diverse observational properties such as size, morphology and line ratios (Abolmasov et al. 2007; Pakull & Mirioni 2003). Integral luminosities in Balmer lines are in some cases of the order 10^{38} erg s^{-1} or higher that requires an energy source with luminosity $\gtrsim 10^{39}$ erg s^{-1} indicating that ULXs are really powerful objects. Therefore strong beaming effects are excluded as the reason of apparently high luminosities of ULXs. For some objects like HoIX X-1 and IC342 X-1 the nebula is clearly shock-powered. In other cases (HoII X-1, M101-P098) low intensity of low-excitation lines, bright [O III] and He II emissions and quiet kinematics¹ suggest photoionization to be the main energy source.

The only proven example of a persistent supercritical accretor is the peculiar binary SS433 (Fabrika 2004). Its accretion rate is of the order 10^{-4} $M_{\odot} \text{yr}^{-1}$, indicating mass transfer on the thermal timescale of a massive star. Most of the accreting material is ejected in the form of optically-thick wind with velocities $V \simeq 1000 - 2000$ km s^{-1} . The total kinetic power of the jets of SS433 is of the order of 10^{39} erg s^{-1} . SS433 is surrounded by a large (roughly 40×120 pc) radionebula W50 (Dubner et al. 1998). The nebula harbors several optical emission-line filaments situated in the propagation direction of the jets. Large difference in angular size and heavy absorption in the case of W50 make comparison with ULXNe difficult.

1.2. NGC6946 ULX-1

The X-ray source under consideration is known as NGC6946 ULX-1 (Swartz et al. 2004), NGC6946 X-8 (Lira et al. 2000), N58 (Holt et al. 2003) or NGC6946 X-11 (Roberts & Colbert 2003). It was first detected by *ROSAT* (Schlegel 1994) and identified with an optical nebula by Blair & Fesen (1994) and a marginally resolved radiosource by van Dyk et al. (1994).

The nebula is known as MF16 – Matonick and Fesen 16 (Matonick & Fesen 1997). It was considered a SNR luminous in X-rays, in fact the most luminous in X-rays among the optically bright SNRs (Dunne et al. 2000), till it was proved by Roberts & Colbert (2003) that the X-ray emission originates from a much more compact source in the center of the nebula. *Chandra* source coordinates for J2000 epoch are: $\alpha = 20^h 35^m 00^s .74$, $\delta = +60^{\circ} 11' 30'' 6$.

The host galaxy NGC6946 is a late-type spiral with active star formation (de Gioia-Eastwood & Grasdalen 1984) and the greatest number of detected supernovae (no less than 8, according to Li et al. (2005)). The distance to the galaxy is estimated by different authors as 5.1 (de Vaucoulers 1978), 5.5 (Tully 1988), 5.7 (Eastman et al. 1996) and 5.5 Mpc (Karachentsev et al. 2000) therefore we assume $D = 5.5$ Mpc. The divergence in distance estimates leads to a 15% uncertainty in all the luminosities inferred. Spatial scale for $D = 5.5$ Mpc is about 27 pc

¹ For HoII X-1 Lehmann et al. (2005) report velocity dispersion ~ 13 km s^{-1} in the vicinity of the X-ray source.

per arcsecond.

A point source in the center of MF16 was detected by Blair et al. (2001) in *HST* data. The source (star **d** as denoted by Blair et al. (2001)) has a V magnitude of $22^m.64$ and a colour index of $B - V = 0^m.46$. The object is significantly redder than the nearby stars **a-c** offset to the North-West by several seconds. If one accounts only for Galactic interstellar extinction (see discussion in section 3.2) equal to $A_V^{(GAL)} = 1^m.14$ according to Schlegel et al. (1998) in the direction of MF16, the point-like counterpart resembles an early A Ia supergiant with $M_V \simeq -7^m$ and $B - V \simeq 0^m$. Additional intrinsic absorption $A_V \sim 0^m.5$ (reported by Blair et al. (2001)) places the object slightly above the Ia sequence in the upper left part of the HR diagram.

Optical emission-line spectrum of the nebula is generally consistent with the suggestion of shock heating but also contains high-excitation lines such as He II λ 4686 and [O III] λ 5007,4959 doublet (Blair & Fesen 1994; Blair et al. 2001) too intensive for optically-bright SNRs (Matonick et al. 1997). Partially radiative shocks were proposed to explain the emission-line spectrum of MF16 (Blair et al. 2001) but they require a very powerful energy source (see discussion in section 4).

The object is much brighter in the optical than a usual SNR. Its H α luminosity is about 2×10^{38} erg s $^{-1}$, an order of magnitude higher than the upper limiting H α luminosity for optically-bright SNRs in nearby galaxies (Braun & Walterbos 1993). Dunne et al. (2000) detected two-component structure in the emission lines of the object in high-resolution echelle spectra. Broader components suggest expansion velocities about 250 km s $^{-1}$, narrower components have velocity dispersion $\sim 20 - 40$ km s $^{-1}$.

MF16 is also known as a radio source as bright as 1.3mJy at 20cm (van Dyk et al. 1994) marginally resolved by VLA observations as a $\sim 1''$ size object. The radio source appears to be displaced relative to the X-ray object and the optical source **d** by $\sim 0''.5$ (see figure 1). Luminosity of the radio counterpart is about 20 times higher than that of W50 at 20cm (Dubner et al. 1998). The size of the radiosource is poorly known but the optical nebula is about 5 times more compact than W50.

MF16 is practically isolated from other HII regions. The nearest one with comparable brightness is situated about 200 pc away (Blair et al. 2001). The inner brighter part of the nebula has a shape of a shell $20 \text{ pc} \times 34 \text{ pc}$ elongated in East to West direction with a brighter Western loop. In the deep *HST* images a faint asymmetric halo may be seen (Blair et al. 2001).

In the following section we describe the observational data. In section 3 we present the results of spectral analysis. In section 4 we analyze the excitation and ionization sources of the nebula and model the observed spectrum using *Cloudy*. In section 5 we discuss our results and the perspectives of UV observations of ULXs.

2. Observations and Data Reduction

All the data were obtained at the Russian SAO 6m telescope. The main information about the observational material is listed in table 1.

The data were flat-fielded and wavelength-corrected. Wavelength calibration was made using a He-Ne-Ar lamp. Atmospheric extinction was corrected using the data obtained by Kartasheva & Chunakova (1978) fitted by a simple formula $\Delta m = (0.013(\lambda/10^4 \text{ \AA})^{-4} + 0.13)\text{sec } z$.

2.1. Integral-Field Spectroscopy

The MultiPupil Fiber Spectrograph (MPFS) is described in Afanasiev et al. (2001). MPFS is a panoramic spectrograph with $16'' \times 16''$ field of view consisting of $256 1'' \times 1''$ spatial sampling elements. Spectra from individual elements arranged according to their coverage of the celestial sphere form a three-dimensional structure that is usually called a data cube. Extra 17 fibers collect sky background from $4'$ away offset regions.

Data reduction system was developed in IDL environment. The reduction process includes the procedures standard for panoramic spectroscopy data reduction (see for example Sánchez (2006)): bias subtraction, cosmic hits removal, flat-fielding, individual fiber extraction, wavelength and flux calibrations. The dispersion curve has an accuracy of about $5 - 10 \text{ km s}^{-1}$. Wavelength shifts between different fibers were corrected using the brightest night sky lines [OI] $\lambda\lambda 5577, 6300, 6364$. We used GD248 spectrophotometric standard (Oke 1990) for flux calibration. Sensitivity variations of individual fibers were corrected using twilight sky exposures.

We also added atmospheric dispersion (or atmospheric differential refraction, ADR) correction with accuracy better than $0''.1$ in order to achieve correct relative astrometry for the datacube. We determined the value of ADR using the spectral standard star. Its shift along the vertical as a function of wavelength was approximated by a second-order polynomial that resulted in a roughly $0''.1$ scatter around the best-fit parabola and no detectable systematical deviations. The spectral standard was observed at different zenith distance ($z_{star} \simeq 40^\circ$, $z_{obj} \simeq 55^\circ$) but we corrected for that difference using the well-checked $\propto \tan z$ dependence for ADR. According to Filippenko (1982) $\propto \tan z$ approximation holds within $\sim 0.2\%$ at the 2 km altitude in the optical range up to $\text{sec } z \sim 5$ ($z \sim 80 \text{ deg}$).

2.2. Long-Slit Spectroscopy

The observations were held with SCORPIO focal reducer (Afanasiev & Moiseev 2005), in the long-slit mode with moderate spectral resolution and slit width $1''$. The position angle ($PA = 96^\circ.5$) of the slit was chosen along the major axis of the nebula (figure 1). Reduction was performed in IDL environment and includes all the standard reduction steps for long-slit spectroscopy.

The signal-to-noise ratio for the long-slit data is about factor 2-3 higher than in the MPFS data, mainly because of the better spectrograph transparency. Integral field data, how-

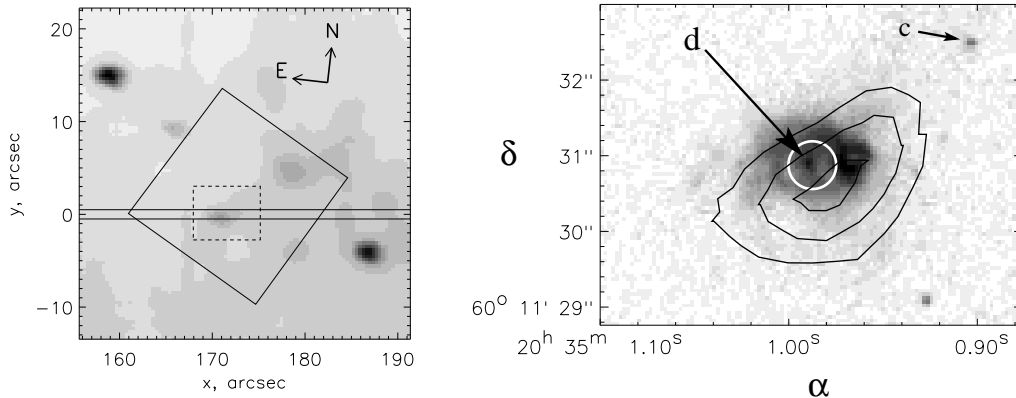


Fig. 1. V-band image obtained during the observations with SCORPIO (on the left panel) and HST ACS archival image (F658N filter) of the source vicinity (right panel, the region is shown on the left panel by a dashed rectangle). MPFS field is shown by a square. Slit position is shown on the left panel by two horizontal lines. Point sources **c** and **d** are marked. White circle is centered at the position of the X-ray source, black contours correspond to the VLA radio isophotes at 4.86GHz (van Dyk et al. 1994).

ever, have the advantage of giving flux values free from slit losses and radial velocities without systematical errors usual for long-slit spectroscopy. Besides this, MPFS data cover larger spectral range.

3. Spectroscopy Results

3.1. Emission Line Spectrum

MPFS spectrum was extracted within $2''$ radius diaphragm, the long-slit spectrum was integrated within a $\pm 1''.5$ band. Emission line fluxes were calculated using gauss analysis. Fitting with two gaussians was used for [SII] $\lambda\lambda 6717, 6731$ doublet, $H\gamma + [\text{OIII}]\lambda 4363$, $\text{HeII}\lambda 4686 + \text{FeIII}\lambda 4658$ and $\text{FeII} + \text{FeIII}\lambda 5262, 5270$ blends and line groups. Triple gaussian was used to deblend $H\alpha$ with [NII] $\lambda 6548, 6583$ doublet (for the components of the latter fixed wavelength difference and flux ratio $F(\lambda 6583/\lambda 6548) = 3$ were adopted). Exact (accuracy $\sim 0.1 \text{ \AA}$ or better) wavelengths were taken from Coluzzi (1996).

Table 2 lists the parameters of all the detected emission lines in the extracted spectra. All the lines redward of 5700 \AA are from the MPFS data, most of the bluer lines have fluxes measured with SCORPIO. Radial velocities from the panoramic data are given when possible. Number of lines such as [N I] $\lambda 5200$ and [S II] $\lambda 4068$ are close doublets or blends with unknown component ratios and therefore may have biased radial velocities by several tens of km s^{-1} . Errors in table 2 give the uncertainties of gaussian parameters. Signal-to-noise ratio is $S/N \sim 3$ for the faintest lines identified like $\text{Fe III}\lambda 4936$. All the fluxes in the second column are normalized over the integral $H\beta$ flux in the corresponding spectrum, and unreddened fluxes

over the unreddened $H\beta$ flux value. Total flux from the MPFS data is $F(H\beta) = (4.66 \pm 0.13) \times 10^{-15}$ erg cm $^{-2}$ s $^{-1}$. Unreddened values are calculated using the reddening curve by Cardelli et al. (1998) with $R_V = 3.1$ and the interstellar extinction value $A_V = 1^m.54$ calculated in section 3.2. Unreddened $H\beta$ flux is $F_{(unreddened)}(H\beta) = (2.50 \pm 0.07) \times 10^{-14}$ erg cm $^{-2}$ s $^{-1}$.

Single strong lines show non-gaussian profiles possibly broadened by kinematical effects of the order 200 km s $^{-1}$. We however lack spectral resolution to deblend the broad and narrow components detected by Dunne et al. (2000). Some of the line identifications are debatable, mostly for weaker lines. However, we definitely see a number of high-excitation emissions like Pickering He II λ 5412 and two putative [Ar IV] lines. Lines of moderately high excitation like He I, Fe III and S III dominate in number among the weaker lines. Some of the emissions are forbidden and therefore of nebular origin. FWHM of the He II λ 4686 emission does not differ significantly from these of the brightest nebular lines like [O III] λ 4959,5007 hence He II λ 4686 is likely to be a nebular emission as well. Stellar or accretion disc emission is expected to be broadened by about 1000 km s $^{-1}$ (Hamann et al. 1995). Wolf-Rayet N III-N IV and CIII/CIV blends at about 4640 Å are definitely absent (at least fainter than the Fe III λ 4658 emission) also supporting nebular origin of the He II λ 4686 emission.

3.2. Characteristic Line Ratios

$H\alpha/H\beta$ flux ratio is commonly used as a probe for interstellar absorption because of its very little dependence on all the plasma parameters. The ratio is nearly constant and equal to 3 with $\sim 10\%$ accuracy in the 5000 – 20000 K temperature and $1 - 10^4$ cm $^{-3}$ number density range for photoionized plasma. We used Cardelli et al. (1998) extinction curve with $R = 3.1$. The integral MPFS spectrum gives $A_V = 1^m.34$ that is slightly greater than the Galactic absorption $A_V^{Gal} = 1^m.14$ in the X-ray source direction (Schlegel et al. 1998). $H\alpha/H\beta$ ratio might be higher than 3 (Dopita & Sutherland 2003) in case of collisional excitation. The effect may be important, for example, for shock waves of moderate velocities $V_S \lesssim 100$ km s $^{-1}$ (Shull & McKee 1979), but its impact is questionable and virtually unstudied. Using the electron temperature and density estimates calculated below this section ($T \simeq 15000$ K, $n_e \simeq 600$ cm $^{-3}$) one arrives to a slightly lower $H\alpha/H\beta$ ratio ~ 2.8 that corresponds to $A_V \simeq 1^m.54$ rather than the value stated above.

Previous spectral studies of MF16 by Blair & Fesen (1994) and Blair et al. (2001) report higher values of interstellar absorption: $E(B - V) = 0.52$ (implying $A_V \simeq 1^m.6$) and $E(B - V) = 0.65$ ($A_V \simeq 1^m.8$), correspondingly. Possible explanation is in patchy extinction making the $H\alpha/H\beta$ flux ratio variable within the extent of the nebula. This is consistent with the relatively low intrinsic absorption (intrinsic colour excess $E(B - V) \lesssim 0^m.1$, implying $A_V \lesssim 0^m.3$) estimated for nearby stars **a-c** (Blair et al. 2001) and high absorbing column obtained for the X-ray source by Roberts & Colbert (2003) $N_H \sim 4 \times 10^{21}$ cm $^{-2}$ corresponding to $A_V \sim 1^m.8$ (Gorenstein 1975).

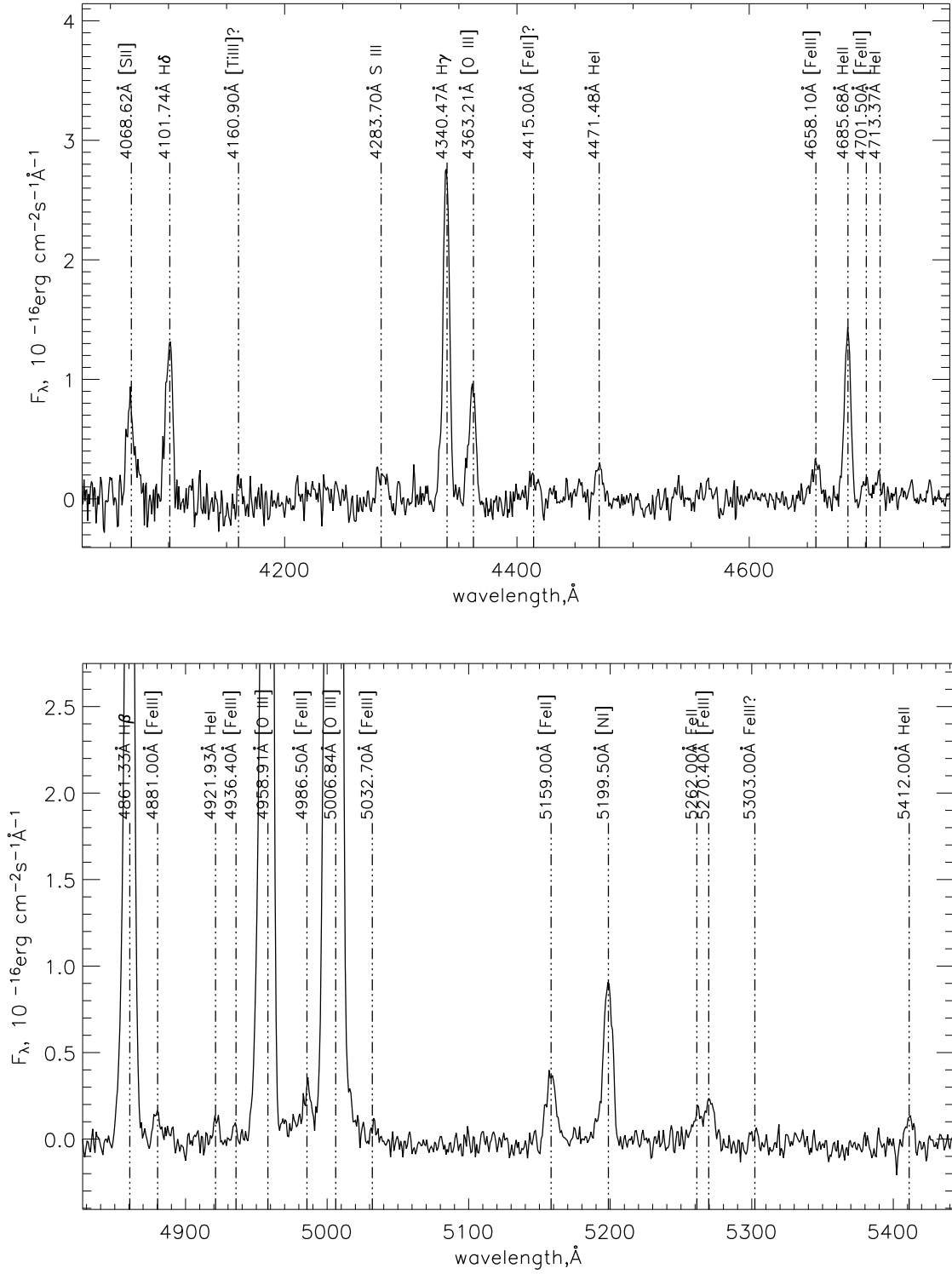


Fig. 2. MF16 integral spectra extracted from the SCORPIO long-slit data.

In order to probe the physical conditions in the nebula we used several characteristic emission line ratios. Characteristic line calibrations were made according to Osterbrock & Ferland (2006) and *STSDAS* on-line *NEBULAR.temden* resource at <http://stsdas.stsci.edu/nebular/temden.html>.

[S II] 6717 / 6731 intensity ratio is usually used for electron density estimates. Integral line flux ratio (1.05 ± 0.03) indicates a rather high value, $n_e = 570 \pm 60 \text{cm}^{-3}$ if one assumes $T = 15000 \text{K}$ (see below). The electron temperature is usually estimated using two characteristic line ratios: [O III] ($\lambda 4959 + \lambda 5007$) / $\lambda 4363$ and [N II] ($\lambda 6548 + \lambda 6583$) / $\lambda 5755$. For different ions we estimate electron temperature as: $T([\text{O III}]) = 17700 \pm 1200 \text{K}$, $T([\text{N II}]) = 15600 \pm 2000 \text{K}$. Somewhat hotter temperatures inferred from [O III] lines are quite reasonable, because [O III] has higher ionization potential and emits in regions with higher temperature. An estimate for the coldest regions of the nebula may be made using [S II] ($\lambda 4068 + \lambda 4076$) / ($\lambda 6717 + \lambda 6731$) flux ratio. Using *temden* we arrive to a temperature estimate $T([\text{S II}]) = 8600 \pm 500 \text{K}$. Large wavelength difference makes this value less defined due to uncertainty in the interstellar absorption value, $T([\text{S II}]) = 9000 \pm 1000 \text{K}$. Here, absorption uncertainty $\sim 0^m.2$ results in about 12% flux ratio uncertainty for the temperature-sensitive doublets of [S II] making total flux ratio uncertainty about two times higher. Accurate temperature determination is limited by the variable absorption effects mentioned above.

Total luminosity of the nebula in the $\text{H}\beta$ emission line may be used to estimate the emission measure and the total mass of the emitting gas. If one assumes constant density and temperature of the order $(1 - 2) \times 10^4 \text{K}$ for all the ionized material the mass of the nebula may be expressed as follows:

$$M \simeq \frac{mEM}{n_e E(\text{H}\beta)} \simeq \frac{mL(\text{H}\beta)}{\alpha^{eff}(\text{H}\beta)n_e E(\text{H}\beta)}, \quad (1)$$

where m is the mean particle mass and α^{eff} is the effective (Case B) recombination coefficient. $L(\text{H}\beta) = (9.0 \pm 0.2) \times 10^{37} \text{ erg s}^{-1}$ is the object luminosity in $\text{H}\beta$. Using the estimates for $n_e = 600 \text{cm}^{-2}$ and $T_e = 15000 \text{K}$ one yields for the case of MF16 $M = 870 \pm 50 M_\odot$, about two times higher than the value obtained by Blair et al. (2001) because of higher $\text{H}\beta$ luminosity inferred. That is similar to the mass of the shovelled material for a spherical nebula with $R = 13 \text{ pc}$ and original interstellar hydrogen density $n_0 \simeq 6 \text{cm}^{-3}$.

4. Ionization sources

4.1. Shock Excitation

Most of the observational properties of MF16 such as two-component emission lines (Dunne et al. 2000), morphology (Blair et al. 2001) and high [S II] $\lambda\lambda 6717, 6731 / \text{H}\alpha$ flux ratio favour shock excitation. Dopita & Sutherland (1996) provide a useful formula for the total flux emerging from a unit radiative shock front surface area in $\text{H}\beta$ (both for the post-shock flow and for precursor):

$$\begin{aligned}
F_{H\beta} &= F_{H\beta,shock} + F_{H\beta,precursor} = \\
&\left(7.44 \times 10^{-6} \left(\frac{V}{100 \text{ km s}^{-1}} \right)^{2.41} + \right. \\
&\left. + 9.86 \times 10^{-6} \left(\frac{V}{100 \text{ km s}^{-1}} \right)^{2.28} \right) \times \\
&\times \frac{n_0}{1 \text{ cm}^{-3}} \text{ erg cm}^{-2} \text{ s}^{-1}
\end{aligned} \tag{2}$$

Here n_0 is the pre-shock hydrogen density and V is the shock velocity in 100 km s^{-1} units. The estimates are supposed to be valid for shock velocities of the order $100 - 1000 \text{ km s}^{-1}$ and densities usual for the ISM and nebulae ($0.1 - 10^4 \text{ cm}^{-3}$). Precursor emission (the second term in brackets) is present only for shock velocities $V_S \gtrsim 150 \text{ km s}^{-1}$ because slower shocks are unable to produce an ionization front moving fast enough (Dopita & Sutherland 2003).

Integrating (2) over shock fronts gives total $H\beta$ luminosities that may be compared with the observed luminosity of the emission-line object. The integral unreddened $H\beta$ luminosity following from the 3D data analysis (see section 3.1) is $L(H\beta) = (9.0 \pm 0.2) \times 10^{37} \text{ erg s}^{-1}$ or $(2.50 \pm 0.07) \times 10^{-14} \text{ erg cm}^{-2} \text{ s}^{-1}$ in flux units. Formula (2) may be rewritten as:

$$\begin{aligned}
F(H\beta) &= \left(2.0 \left(\frac{V}{250 \text{ km s}^{-1}} \right)^{2.41} + \right. \\
&\left. + 2.4 \left(\frac{V}{250 \text{ km s}^{-1}} \right)^{2.28} \right) \frac{n_0}{5 \text{ cm}^{-3}} \theta^2 \times \\
&\times 10^{-15} \text{ erg cm}^{-2} \text{ s}^{-1}
\end{aligned} \tag{3}$$

θ is the angular diameter of the nebula in arcseconds. The estimate (3) predicts $H\beta$ flux several times less than the observed value. Shock waves are short in producing enough flux in $H\beta$ unless the initial density $n_0 > 10 \text{ cm}^{-3}$ (that is unlikely because the mass of the shocked material should be much higher than the mass of the emitting gas) or the shock velocity $\gtrsim 300 \text{ km s}^{-1}$ (that is excluded by kinematical data). Besides this, observed intensities of [O III] and [N II] lines require shock with $V_S \sim 300 - 400 \text{ km s}^{-1}$ (Dopita & Sutherland 1996; Evans et al. 1999) that is significantly higher than what one may allow having the kinematical limits mentioned above. He II λ 4686 emission line is much brighter with respect to $H\beta$ than a shock wave with precursor with $V_S < 1000 \text{ km s}^{-1}$ can provide (Evans et al. 1999). We conclude that observed expansion velocities are too low to explain the emission line luminosities observed as well as the line ratios.

4.2. Photoionization

An evident solution is to consider a bright photoionizing source that can increase the total luminosity in $H\beta$ without changing the line widths. One may suggest the X-ray radiation of the central source responsible for powering the nebula. In order to check the ability of the X-ray source to power the nebula we set the radius of the nebula equal to 13pc (according to Blair et al. (2001)) and used the best-fit MCD + power-law model from Roberts & Colbert (2003). MCD (MultiColour Disc blackbody) was calculated according to Mitsuda et al. (1984). Soft MCD component was extrapolated to the EUV region, but we truncated the power-law at 0.5 keV where its intensity becomes comparable with that of the MCD component.

The observed X-ray radiation provides an ionization parameter logarithm $\lg U \simeq -5.2$ ². However, observed $[\text{O III}]\lambda 5007/\text{H}\beta \sim 7$ and $\text{He II}\lambda 4686/\text{H}\beta \sim 0.2$ ratios point to a rather high ionization parameter logarithm value $\lg U \gtrsim -3$ (Evans et al. 1999). Besides this, as we see below, the X-ray source itself is unable to produce enough photoionizing quanta. This can be done by introducing a powerful extreme ultraviolet (EUV) source ($L_{\text{EUV}} \sim 10^{40}$ erg s⁻¹).

He II $\lambda 4686$ emission line is much brighter with respect to H β than a shock wave with reasonable parameters may explain. Total luminosity in the line is $L_{\text{He II}\lambda 4686} = (2.0 \pm 0.2) \times 10^{37}$ erg s⁻¹ according to the MPFS data. Because of this and the high excitation potential of the corresponding transition, we consider He II $\lambda 4686$ a recombination line. One can estimate the number of ionizing quanta required and the luminosity of the photoionizing source following Osterbrock & Ferland (2006) (Zanstra method):

$$Q(\text{He}^+) \geq \frac{1}{E(\lambda 4686)} \times \times \frac{\alpha_B}{\alpha^{eff}(\text{He II}\lambda 4686)} L(\text{He II}\lambda 4686), \quad (4)$$

α_B and $\alpha^{eff}(\text{He II}\lambda 4686)$ here are the total recombination rate for the Case B and the effective recombination rate for the He II $\lambda 4686$ line (Osterbrock & Ferland 2006), correspondingly. Their ratio depends weakly on plasma parameters, varying by a factor of 2 in the plasma temperature range $(1 - 30) \times 10^3$ K. For particle density of the order $100 - 1000$ cm⁻³ and temperature $T \sim (1.5 - 2) \times 10^4$ K the recombination coefficient ratio $\alpha_B/\alpha^{eff}(\text{He II}\lambda 4686) \simeq 4.7$. Corresponding luminosity of the He⁺-ionizing EUV source is $L(\lambda < 228 \text{ \AA}) \gtrsim 95L(\text{He II}\lambda 4686) \simeq 2 \times 10^{39}$ erg s⁻¹. Note that all the ionizing luminosity must be concentrated in the wavelength range $20 - 200 \text{ \AA}$ (at $\lambda \lesssim 20 \text{ \AA}$ heavier elements dominate the extinction). The luminosity is calculated for $\lambda = 228 \text{ \AA}$ and actually is a lower estimate because of higher photon energies and quanta leakage. Though bright He II $\lambda 4686$ emission seems to be quite usual for ULX counterparts (Abolmasov et al. 2007), for MF16 the He II luminosity is extremely large. The EUV luminosity inferred is comparable with the X-ray luminosity.

Similar estimates may be made for other recombination lines such as H β and He I $\lambda 4471$. The Case B numbers of He⁺, He⁰ and H⁰-ionizing quanta derived from He II $\lambda 4686$, He I $\lambda 4471$ and H β , correspondingly, are as follows:

$$Q(\text{He}^+) = (2.2 \pm 0.2) \times 10^{49} \frac{L(\text{He II}\lambda 4686)}{2.0 \times 10^{37} \text{ erg s}^{-1}} \text{ s}^{-1} \quad (5)$$

$$Q(\text{He}^0) = (1.8 \pm 0.2) \times 10^{49} \frac{L(\text{He I}\lambda 4471)}{4.0 \times 10^{36} \text{ erg s}^{-1}} \text{ s}^{-1} \quad (6)$$

$$Q(\text{H}^0) = (1.90 \pm 0.05) \times 10^{50} \frac{L(\text{H}\beta)}{9.0 \times 10^{37} \text{ erg s}^{-1}} \text{ s}^{-1} \quad (7)$$

² Here and below we define ionization parameter as (following Evans et al. 1999):

$$U = \frac{1}{cn_H} \int_{13.6\text{eV}}^{+\infty} \frac{F_\nu}{h\nu} d(h\nu),$$

where n_H is the total (ionized + neutral + molecular) hydrogen density in the gas.

The ionizing quanta numbers listed above correspond to ionizing source luminosities greater than 10^{39} erg s⁻¹. Luminosity required to explain the $H\beta$ luminosity of MF16 is $L(\lambda < 912 \text{ \AA}) \gtrsim 4 \times 10^{39}$ erg s⁻¹.

4.3. Photoionization grid

We have computed a grid of *Cloudy* version 07.02.00 (Ferland et al. 1998) photoionization models in order to fit the spectrum of MF16 neglecting shock waves. We assumed all the plasma situated at 13 pc from the point source in the center, forming a hollow envelope with hydrogen density $n_H = 500 \text{ cm}^{-3}$. We considered photoionization with an isotropic source with a two-component spectrum: fixed X-ray component observed by *Chandra* (and extrapolated in the EUV region in the same way it was done in the previous section) and a blackbody source with the temperature spanning the range from 10^3 to 10^6 K and integral flux densities from 0.01 to $100 \text{ erg cm}^{-2} \text{ s}^{-1}$ (corresponding to the luminosity range $10^{37} - 10^{41}$ erg s⁻¹).

8 lines with different ionization potentials were used for fitting. Measured emission line fluxes were fitted assuming the distance $D = 5.5$ pc. Two interstellar extinction values were applied, $A_V = 1^m.34$ and $1^m.54$, the latter resulting in much better fit supporting the idea that the flux ratio $H\alpha / H\beta \simeq 2.8$ rather than 3. Fitting results and partial χ^2 values are given in table 3.

The best-fit parameters for MF16 are: $\lg T(K) = 5.15 \pm 0.10$, $F = 0.6 \pm 0.1 \text{ erg cm}^{-2} \text{ s}^{-1}$ resulting in a normalized $\chi^2 \simeq 25$ (for 6 degrees of freedom). The luminosity of the corresponding UV source is $L_{UV} \simeq 1.2 \times 10^{40}$ erg s⁻¹ (mainly concentrated at 200 – 400 Å). The high values of the reduced χ^2 are a direct result of the high S/N in our data. Note that all the line fluxes are predicted with the accuracy better than $\sim 20\%$ quite reasonable for our analysis. All the line ratios are affected by plasma inhomogeneities, abundance and depletion effects. In principle a more complicated model may be applied to our data. Hotter lines like He II λ 5412 and [O III] λ 4363 are enhanced in the observed spectrum with respect to the best-fit photoionization model predictions indicating an additional source of heating. Model [O III] temperature is about 10^4 K instead of 1.7×10^4 K measured from the [O III] characteristic line ratio.

Our models also overestimate the intensities of Fe III lines. This may be attributed to partial depletion of the element into dust taking place in the interstellar medium. Iron depletion values are usually of the order 10^{-2} for undisturbed dense ISM and about 0.1 for HII-regions (Rodríguez 2002) indicating that dust is effectively destroyed in MF16. Shock waves are likely to destroy significant part of dust grains in the ISM but some percentage of grains survive for $V_S \lesssim 500 \text{ km s}^{-1}$ (Dopita & Sutherland 2003; Jones et al. 1994). The rich spectrum of Fe III indicates that the emitting gas was processed by shock waves showing however depletion by a factor of 0.3 – 0.5.

We conclude that the observed emission-line spectrum may be reproduced without any significant abundance changes and without shock waves. However, the effect of the latter may

still be important (in heating the medium and destroying dust).

5. Discussion

5.1. The Nature of the EUV Source

Cool multicolour disc (MCD) + power law models are often used to fit ULX spectra and are considered an argument for the IMBH model (Colbert & Miller 2005). Hard power law component usually dominates the X-ray spectrum but it is expected to be truncated at energies close to the inner disc temperature. For NGC6946 ULX-1 about 20% of the standard *Chandra* X-rays may be attributed to the thermal MCD component with the inner temperature $T_{in} = 0.15$ keV (Roberts & Colbert 2003). Bolometric luminosity of a standard disc with such a temperature should be about 5 times higher than its luminosity in the standard *Chandra* X-ray range. Though most of the disc luminosity is emitted in the EUV range the number of photons is insufficient to explain the Balmer lines. It may be checked that a conventional MCD with the parameters measured by *Chandra* provides only $Q_H \simeq 10^{49} \text{ s}^{-1}$ – at least an order of magnitude less than is needed to explain the $H\beta$ luminosity. Luminosity of the He II $\lambda 4686$ line is however only about 2 times higher than the MCD component can provide.

The central optical point source (star **d** in figure 1) is much brighter than a possible low-energy tail of a standard accretion disc. According to Blair et al. (2001), star **d** has $V = 22^m.64$ and $B - V = 0^m.46$. For a distance of 5.5 Mpc and $A_V = 1^m.54$ the central optical point-like source will have $M_V = -7^m.6$ ($L_V \sim 3 \times 10^{38} \text{ erg s}^{-1}$) instead of $M_V = -2^m.7$ given by the best-fit MCD for *Chandra* data with an infinite outer radius. The optical excess, however, may be attributed to the donor star. The optical object itself is relatively cool: $(B - V)_0 \simeq -0^m.05$ if one assumes colour excess following from the A_V estimates due to $H\alpha/H\beta$ ratio $E(B - V) \simeq A_V/3.1 \simeq 0.5$. That corresponds to a temperature $\sim 10^4 \text{ K}$. Exponentially small part ($\exp\{-Ry/T\} \sim 4 \times 10^{-5}$) of the photons emitted by the star is able to ionize hydrogen and helium, therefore the contribution of the donor star to the ionization balance in MF16 is probably negligible. About 1^m additional intrinsic absorption is needed to make the optical source a hot blackbody with $B - V \sim -0.3^m$.

In figure 3 we reconstruct the spectral energy distribution (SED) of the ULX throughout the UV spectral range (from X-rays to the optical). Our estimates of ionizing luminosities put together with the X-ray best-fit model spectrum (Roberts & Colbert 2003) result in a source with an approximately flat ($\nu L_\nu \sim \text{const}$) spectrum from 0.01 to 10 keV. Ionizing flux estimates (5-7) are indeed lower limits due to higher energies of the absorbed quanta and possible quanta leakage. The estimated EUV luminosity can not be explained by an MCD with $T_{in} \sim 0.1 - 0.2$ keV. In figure 3 we show MCD spectra for different black hole masses (10, 100, 1000 and 10000 M_\odot from bottom left to top right) accreting at 1% of the critical accretion rate.

For a standard disc (Shakura & Sunyaev 1973) luminosity and temperature scale with

the black hole mass M and dimensionless accretion rate \dot{m} as $L \propto M\dot{m}$, $T_{in} \propto M^{-1/4}\dot{m}^{1/4}$, correspondingly. Mass and accretion rate estimates are therefore much more sensitive to the SED shape than to luminosity: $M \propto L^{1/2}T_{in}^{-2}$, $\dot{m} \propto L^{1/2}T_{in}^2$. The black hole mass in the framework of the IMBH hypothesis should be $\sim (1 - 3) \times 10^4 M_\odot$.

Our best-fit model parameters (section 4.3) suggest an object with radius $\sim 10 R_\odot$ and temperature $\sim 10^5$ K too high even for a conventional Wolf-Rayet star. Hot WC and WO stars may have comparable effective temperatures, but their luminosities and ionizing quanta production rates are at least an order of magnitude lower (Crowther et al. 2006). A possible interpretation is emission from the optically thick wind of a supercritically accreting stellar mass black hole that should be a bright UV/EUV source of appropriate luminosity (Poutanen et al. 2007). The X-ray component may be attributed to the funnel radiation in that case. Poutanen et al. (2007) estimate the outer photosphere temperature of a supercritical accretion disc wind as:

$$T_{ph} \simeq 0.8m^{-1/4}\dot{m}^{-3/4} \text{ keV} \quad (8)$$

where m is the black hole mass in solar units, \dot{m} is the dimensionless mass accretion rate at the infinity. From the equation (8) the dimensionless mass accretion rate may be estimated as $\dot{m} \simeq 200m_1^{-1/3}T_5^{-4/3}$, where m_1 is the black hole mass in $10 M_\odot$ units, and T_5 is the temperature of the photosphere of the wind in 10^5 K. The accretion (or, more strictly, mass ejection) rate is found to be about an order of magnitude less than expected for SS433 (Fabrika 2004) yet still highly supercritical.

5.2. ULXs in the UV

Let us assume the SED of the central object smooth throughout the UV range and interpolate between the optical and EUV flux estimates with a power-law (see figure 3). The predicted intrinsic (unabsorbed) flux at 1000 \AA is $F_\lambda \sim 10^{-15} \text{ erg cm}^{-2} \text{ s}^{-1} \text{ \AA}^{-1}$. At shorter wavelengths radiation is highly absorbed by neutral gas. Absorption by dust at $\lambda \sim 1000 - 2000 \text{ \AA}$ may be estimated as about $(3 - 4) \times A_V \sim 5^m$ (Cardelli et al. 1998), so one should expect at 1000 \AA $F_\lambda \sim 10^{-17} \text{ erg cm}^{-2} \text{ s}^{-1} \text{ \AA}^{-1}$, that corresponds to $m_{AB} \sim 25^m$ (we use m_{AB} definition from Oke & Gunn 1983).

Predicted UV flux is quite reachable for *GALEX* pointing observations but too faint to be detected in the All-sky and Medium-sky imaging surveys (Martin et al. 2005) mainly because of high interstellar absorption in UV spectral range. Less absorbed ULXs might be quite achievable targets if they are as bright as NGC6946 ULX-1 in the UV. In figure 3 we compare the νF_ν values with flux limits (10^5 s, $S/N = 5$) for *GALEX* photometry in FUV (1400-1700 \AA) and NUV (2000-2700 \AA) bands. Signal-to-noise estimates were made with the *GALEX* Exposure Time Calculator (<http://kaweah.caltech.edu:8000/ExpCalc.tcl>).

Capabilities of the *HST* instrumentation may be used as well to study ULX sources, at least those less absorbed than NGC6946 ULX-1. Liu et al. (2005) studied the UV counterpart

of NGC5204 X-1 (U1 object) with STIS MAMA in the FUV range and classified the UV object as a B0Ia star with some oddities like strong NV λ 1240 emission that may be attributed to an ambient HII region, irradiated accretion disc or corona. Some resonance lines like SiIV λ 1400 and CIV λ 1550 that show P Cygni-type profiles in OB supergiant spectra are missing (or present only as weak absorptions) in the spectra. Liu et al. (2005) explain this effect by Roche lobe overflow by the B supergiant donor star in a binary system. This argumentation seems to be questionable because the winds of early B-stars have terminal velocities about 1000 km s⁻¹, an order of magnitude higher than virial velocities characteristic for HMXBs. There is however an alternative explanation for the unusual absorption spectrum of U1: P Cygni profiles of UV lines formed in hot rarefied atmospheres of OB Ia/b supergiants transform into absorptions with increasing mass loss (Hutchings 1976). Mass loss rate needed for these effects to become important is of the order 10⁻⁴ M_⊙yr⁻¹. It is also possible that the OB-supergiant spectrum originates not from the donor star but from the accretion disc wind atmosphere, that is probable if the mass accretion rate is close to that observed in SS433.

Monochromatic flux at 2200 Å reported by Liu et al. (2005) for U1 is $F_{\lambda} \simeq 3.7 \times 10^{-17}$ erg cm⁻² s⁻¹ Å. The best-fit absorbing column measured for the X-ray source implies $E(B - V) = 0^m.28$. Galactic absorption is negligibly small ($E(B - V) = 0^m.013$ according to Schlegel et al. (1998)). Intrinsic UV luminosity of NGC5204 X-1 calculated using these values appears to be $\nu L_{\nu} \sim 10^{38}$ erg s⁻¹ not taking into account absorption or $\sim 10^{39}$ erg s⁻¹ if reddening calculated from X-ray fitting is used.

Unfortunately, STIS stopped science operation in 2004 and its potential for studying ULXs in the UV was lost. ACS SBC and HRC cameras require exposures $\gtrsim 10^5$ s to obtain $S/N \gtrsim 1$ (exposure time calculator at http://apt.stsci.edu/webetc/acs/acs_img_etc.jsp was used) in the case of NGC6946 ULX-1 but may be used to study less absorbed bright UV counterparts. Among the most perspective ULXs are NGC5204 X-1, NGC4559 X-7 (Soria et al. 2005), HoII X-1 (Lehmann et al. 2005) and HoIX X-1 (Miller 1995) but we do not have any direct evidence that these objects are as bright as NGC6946 ULX-1 (line luminosities are generally lower).

The two most popular models of ULXs (IMBHs and supercritical accretion discs) both predict strong UV/EUV emission. IMBHs are expected to be bright UV sources due to the disc temperature dependence on the mass of the accretor ($T_{in} \propto M^{-1/4}$). The greater is the mass of the black hole the higher is the UV flux, approximately as $F \propto M^{4/3}$ at a given wavelength for fixed dimensionless accretion rate (Shakura & Sunyaev 1973; Mitsuda et al. 1984). Standard accretion discs around IMBHs are expected to be truncated only at very low temperatures, close to 1 eV (if their outer radii are due to tidal truncation; see, for example, discussion in Abolmasov et al. (2007)), and must have therefore a distinguished spectral slope characteristic for an MCD with an infinite outer radius, $F_{\nu} \propto \nu^{1/3}$ (Shakura & Sunyaev 1973).

Advective super-Eddington discs are often fitted by slim disc models (Abramowicz et al. 1988) predicting roughly flat SED in the X-ray band. On the other hand, supercritical

accretion discs are expected to have strong optically thick winds (Shakura & Sunyaev 1973) with photospheres having blackbody-like spectrum peaking somewhere in the EUV/UV region (Poutanen et al. 2007). The exact structure of the accretion flow is irrelevant for the EUV/UV SED because most of the EUV radiation comes from the wind photosphere. In the *GALEX* range the spectrum is expected to have a Rayleigh-Jeans shape $F_\nu \propto \nu^2$.

We conclude that detecting ULXs in the *GALEX* UV range and measuring the spectral slope may help to distinguish between these two models of ULXs (IMBH or supercritical accretion). At least for some subsample of ULXs (those having indications for a hard photoionizing continuum) different models predict different spectral slopes in the UV range (see figure 3).

The nebula may contribute to the UV emission from the source. Cloudy model predicts total flux in the *GALEX* range about an order of magnitude less than that expected from the ULX itself. Best-fit model predicts $L(Ly\alpha) \simeq 26L(H\beta) \simeq 2 \times 10^{39}$ erg s⁻¹ but most of the Ly α -quanta are likely to be absorbed by neutral interstellar medium. Expected contribution from the nebula is shown in figure 3. Higher fluxes may appear if some additional amount of gas with at least comparable emission measure and much higher temperature is present (much cooler gas does not contribute to the continuum in the UV range). But the optical spectra contain no signatures of high-temperature plasma such as coronal lines of very high-ionization element species. Therefore nebular emission is unlikely to give a significant contribution to the *GALEX* UV in the particular case of MF16.

5.3. MF16 as a Jet-Blown Shell

From the high spatial resolution *HST* images (Blair et al. 2001) it can be seen that the nebula is elongated with an axis ratio no less than ~ 1.5 . Either an underlying density gradient or highly anisotropic energy injection in the ISM is needed to explain the observed morphology.

If a shell evolves in a strong density gradient, one side expands with a much higher velocity making the nebula much more extended in one direction than in the other. Central position of the optical star **d** is difficult to explain in this scope. Density gradient probably plays significant role only in making one side of MF16 much brighter. This is expected (Maciejewski & Cox 1999) even for very shallow density gradients.

In all the self-similar solutions usually applied to expanding shells (Lozinaskaya 1992) and wind-blown bubbles (Castor et al. 1975), energy and mechanical luminosity appear with very low exponents. In particular, for the Sedov solution for an adiabatic-stage SNR the radius of the shell depends as $R \propto E^{1/5}$ on the energy input. Therefore to achieve 50% variation in the radius of the nebula, energy injected per unit solid angle (or the initial ISM density) must change no less than by an order of magnitude. However, if the central machine is a source of well-collimated wind or jets, the shape is naturally explained.

Jet activity is unlikely to be present in standard discs (expected in the framework of IMBH model) and may be considered an argument for supercritical accretion. We do see a pair

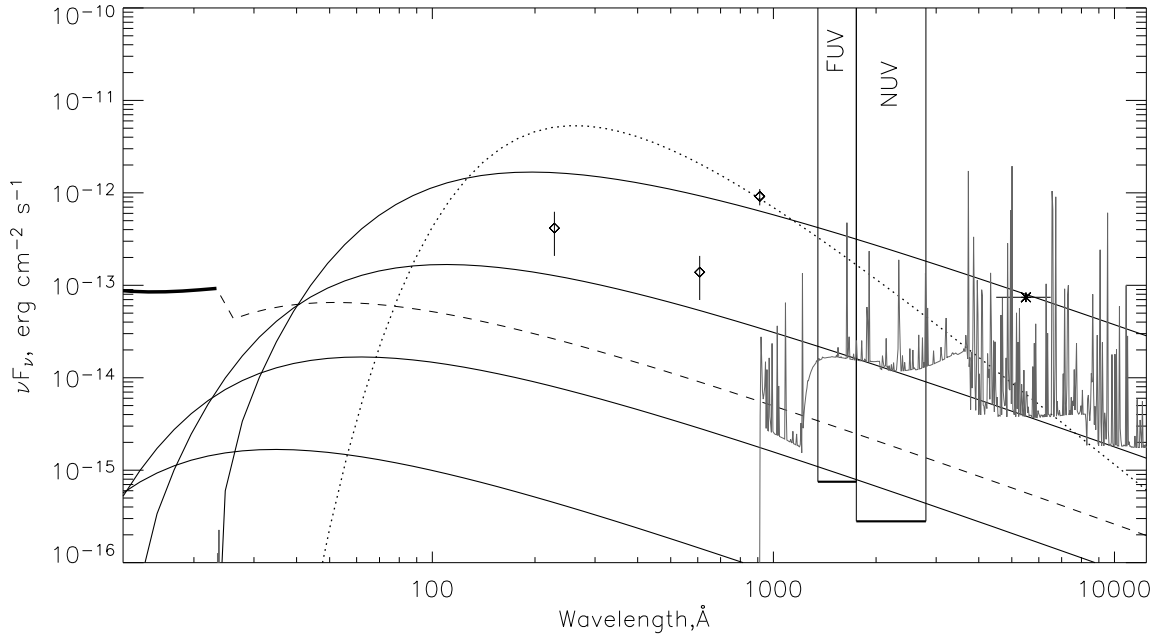


Fig. 3. Reconstructed SED of NGC6946 ULX-1 from X-rays to the optical. Part of the best-fit X-ray spectrum (Roberts & Colbert 2003) is shown by a thick solid line at shorter wavelengths. Dashed curve shows the behavior of the *Chandra* MCD component (outer radius is set to infinity) at longer wavelengths. Ionizing flux estimates for HeII, HeI and HI are shown by diamonds with error bars. Asterisk corresponds to the optical source **d** (Blair et al. 2001) in the V band corrected for interstellar absorption $A_V = 1^m.54$. MCD SEDs are shown (thin solid lines) for $\dot{m} = 0.01$ and masses 10, 100, 1000 and $10^4 M_\odot$. The best-fit black body obtained during our *Cloudy* modelling (see section 4.3) is shown by a dotted line. *GALEX* photometric limits (FUV and NUV bands) are given for S/N=5, exposure time 10^5 s. Gray line shows the best-fit *Cloudy* model spectrum of the nebula.

of powerful jets and an elongated nebula W50 in the case of SS433. However, if NGC6946 ULX-1 is a supercritical accretor viewed face-on (at inclination $i \lesssim 20^\circ$) the direction of jets must be close to the line of sight. In that case the actual length of MF16 should be several times (about $\sin^{-1} i$) greater, approaching the size of W50.

NGC6946 is seen nearly face-on: according to Gordon (1968), its inclination is in the range $16 - 27^\circ$. If the actual size of MF16 in the direction perpendicular to the disc plane of the host galaxy is of the order 100 pc as in the case of W50 then the nebula is likely to evolve in an ISM with a considerable density gradient. The thickness of the gaseous disc in NGC6946 probably does not differ too much from the Galactic neutral hydrogen disc thickness $\simeq 300$ pc (Lockman & Gehman 1991). The expected effects are similar to those observed in the case of W50 that evolves in a strong ISM density gradient (Lockman et al. 2007). It is quite probable that the asymmetry of MF16 seen in *HST* images originates from the interaction of one of the jets with denser material closer to the galactic plane.

6. Conclusions

In our optical spectra of MF16 we detect more than 30 emission lines including several high-excitation lines of He II and [Ar IV] and a rich spectrum of moderately high excitation Fe III lines. He II lines are narrow (broadened by $\lesssim 300 \text{ km s}^{-1}$). We also do not detect any Wolf-Rayet features. Therefore we suggest that the He II λ 4686 line is of nebular origin.

Large intensities of iron lines indicate moderately low depletion of the element into dust (30 – 50% in the gas phase), probably due to dust destruction in shock waves. Destruction is probably incomplete because *Cloudy* models overestimate the intensities of Fe III lines.

We find the electron density in the nebula $n_e = 570 \pm 60 \text{ cm}^{-3}$ ([S II] λ 6717,6731), electron temperatures for different ions are $T(\text{[O III]}) = 17700 \pm 1200 \text{ K}$, $T(\text{[N II]}) = 15600 \pm 2000 \text{ K}$ and $T(\text{[S II]}) = 9000 \pm 1000 \text{ K}$ indicating the presence of regions with different electron temperatures. Total hydrogen emitting gas mass is $M \sim 900 M_\odot$. Interstellar absorption is $A_V \simeq 1^{\text{m}}.34$ in traditional $\text{H}\alpha/\text{H}\beta=3$ assumption. More realistic value $\text{H}\alpha/\text{H}\beta=2.8$ results in a higher extinction value $A_V = 1^{\text{m}}.54$.

The observed line luminosities and diagnostic line ratios appear to be inconsistent with excitation and ionization by shock waves, therefore we suggest an EUV source responsible for powering the nebula. Photoionization modelling with *Cloudy* as well as *Zanstra* estimates suggest the central source must be ultraluminous not only in X-rays but also in the UV/EUV range emitting about $10^{40} \text{ erg s}^{-1}$ in the spectral range 100 – 1000 Å. Using the observed X-ray spectrum, ionizing flux estimates from He II, He I and H lines and the optical point-like counterpart (star **d**) we reconstruct the SED of the central object from X-rays to the optical. The derived spectrum is roughly flat, $\nu L_\nu \sim \text{const}$.

Both most popular models of ULXs (IMBHs and supercritical accretion discs) predict high UV/EUV luminosities. However these two models predict different spectral slopes in the UV region. We conclude that measuring the spectral slope will help to distinguish between the two models as well as to determine the parameters of the successful model such as the black hole mass in the case of IMBH or accretion rate in the case of a supercritical accretion.

Actual excitation and ionization conditions in MF16 may be much more complicated. Though introducing a bright EUV source is a possible way to explain the spectrum, we suggest that other explanations such as high pre-shock density and multiple shocks with different velocities are not completely excluded. Observations with higher angular and spectral resolution (but also higher S/N ratio than that used by Dunne et al. (2000)) may provide additional information about the enigmatic nebula MF16.

We thank V. Afanasiev and N. Borisov for assistance with the observations and the anonymous referee for valuable comments and suggestions. This work was supported by the Russian RFBR grants 06-02-16865 and 07-02-00909 and the RFBR/JSPS grant 05-02-19710. TK is supported by a 21st Century COE Program at Tokyo Tech “Nanometer-Scale Quantum

Physics” by the Ministry of Education, Culture, Sports, Science and Technology. This work is supported by the Japan-Russia Research Cooperative Program of Japan Society for the Promotion of Science.

References

- Abolmasov, P., Fabrika, S., Sholukhova, O. & Afanasiev, V. 2007, *Astrophysical Bulletin*, 62, 36
- Abramowicz, M. A., Czerny, B., Lasota, J. P. & Szuszkiewicz, E. 1988, *ApJ*, 332, 646
- Afanasiev V.L., Dodonov S.N. & Moiseev A.V., 2001, in *Stellar dynamics: from classic to modern*, eds. Osipkov L.P., Nikiforov I.I., Saint Petersburg, 103
- Afanasiev, V. & Moiseev, A., 2005 *Astronomy Letters*, 31, 194
- Blair, W. P. & Fesen, R. A. 1994 *ApJ*, 424, L103
- Blair, W. P., Fesen, R. A. & Schlegel, E. M. 2001 *AJ*, 121, 1497
- Braun, R. & Walterbos, R. A. M. 1993, *ApJS*, 98, 327
- Cardelli, J. A., Clayton, G. C. & Mathis, J. S. 1989 *ApJ*, 345, 245
- Castor, J., McCray, R. & Weaver, R. 1975, *ApJL*, 200, 107
- Colbert, E. J. M. & Miller, E. C., 2005, in *The Tenth Marcel Grossmann Meeting Eds.: Mário Novello; Santiago Perez Bergliaffa; Remo Ruffini*. p.530; astro-ph/0402677
- Coluzzi, R. 1996 *Bull. Inf. Centre Donnees Stellaires*, 48, 15
- Crowther, P. 2007, *ARA&A*, 45, 177
- de Gioia-Eastwood, K. & Grasdalen, G., L. 1984, *ApJ*, 278, 564
- De Vaucouleurs, G. 1978 *ApJ*, 224, 710
- Dolan J. F., Boyd P. T., Fabrika S. et al. 1997 *A&A*, 327, 648
- Dopita, M. A. & Sutherland, R. S. 1996 *ApJS*, 102, 161
- Dopita, M. A. & Sutherland, R. S. “Astrophysics of the diffuse universe” 2003, Berlin, New York: Springer. *Astronomy and astrophysics library*.
- Dubner, G. M., Holdaway, M., Goss, W. M. & Mirabel, I. F. 1998, *ApJ*, 116, 1842
- Dunne, B. C., Gruendl, R. A. & Chu, Y.-H. 2000, *AJ*, 119, 1172
- Eastman, R. G., Schmidt, B. P., & Kirshner, R. 1996, *ApJ*, 466, 911
- Evans, I., Koratkar, A., Allen, M., Dopita, M., Tsvetanov, Z. 1999 *ApJ*, 521, 531
- Fabian, A. C. & Terlevich, R. 1996 *MNRAS*, 280, L5
- Fabrika, S. & Mescheryakov, A., 2001, In *Galaxies and their Constituents at the Highest Angular Resolutions*, Proceedings of IAU Symposium N205, R. T. Schilizzi (Ed.), p. 268, astro-ph/0103070
- Fabrika, S. 2004, *Astrophys. Space Phys. Res.*, 12, 1
- Ferland, G. J. Korista, K.T. Verner, D.A. Ferguson, J.W. Kingdon, J.B. & Verner, E.M. 1998, *PASP*, 110, 761
- Filippenko, A. V. 1982, *PASP*, 94, 721
- Gordon, K. J., Kurtis, N. H. & Roberts, M. S. 1968, *ApJ*, 154, 845
- Gorenstein, P. 1975, *ApJ*, 198, 95
- Hamann, W.-R., Koesterke, L. & Wesselowski, U. 1995, *A&A*, 299, 151
- Holt, S. S., Schlegel, M. E., Hwang, U. & Petre, R. 2003 *ApJ*, 588, 792
- Hutchings, J. B. 1976, *ApJL*, 204, 99
- Jones, A. P., Tielens, A. G. G. M., Hollenbach, D. J. & McKee, C. F. 1994, *ApJ*, 433, 797
- Karachentsev, I. D., Sharina, M. E. & Huchtmeier, W. K. 2000, *A&A*, 362, 544
- Kartasheva, T. A., Chunakova, N. M. 1978, *Astrof. Issled. Izv. Spets. Astr. Obs.*, 10, 44
- Katz, J. I. 1986, *ComAp*, 11, 201

- King, A. R., Davies, M. B., Ward, M. J., Fabbiano, G. & Elvis, M. 2001, *ApJ*, 552, 109
- Körding, E., Falcke, H. & Markoff, S. 2002, *A&A*, 382, 13
- Kuntz, K. D., Gruendl, R. A., Chu, Y.-H. et al. 2005, *ApJL*, 620, 31
- Lehmann, I., Becker, T., Fabrika, S. et al. 2005 *A&A*, 431, 847
- Li, W., van Dyk, S. D., Filippenko, A. V. & Cuillandre, J.-C. 2005, *PASP*, 117, 121
- Lira, P., Lawrence, A. & Johnson, R. A. 2000 *MNRAS*, 319, 17L
- Liu, J.-F., Bregman, J. N. & Seitzer, P. 2004, *ApJ*, 602, 249
- Lockman, F. J., Blundell, K. M. & Goss, W. M. 2007, *MNRAS*, 381, 881
- Lockman, F. J. & Gehman, C. S. 1991 *ApJ*, 382,182
- Lozinskaya, Tatiana A. “Supernovae and stellar wind in the interstellar medium” 1992 New York: American Institute of Physics
- Maciejewski, W. & Cox, D. P. 1999, *ApJ*, 511, 792
- Madau, P. & Rees, M. J. 2001, *ApJL*, 551, 27
- Martin, C. et al., 2005, *ApJ*, 619, 1L
- Matonick, D. M. & Fesen, R. A., 1997 *ApJS*, 112, 49
- Matonick, D. M., Fesen, R. A. & Blair, W. P. 1997 *ApJS*, 113, 333
- Miller, B. W. 1995 *ApJ*, 446, L75-L78
- Mitsuda, K., Inoue, H., Koyama, K. et al. 1984, *PASJ*, 36, 741
- Okajima, T., Ebisawa, K., Kawaguchi, T. 2007, *ApJL*, 652, 105
- Oke, J. B. & Gunn, J. E. 1983, *ApJ*, 266, 713
- Oke, J. B. 1990, *AJ*, 99, 1621
- Osterbrock, D. E. & Ferland, G. “Astrophysics of Gaseous Nebulae and Active Galactic Nuclei” 2006, 2nd. ed. by D.E. Osterbrock and G.J. Ferland. Sausalito, CA: University Science Books, 2006
- Pakull, M. W. & Mirioni, L. 2003 *RevMexAA (Serie de Conferencias)*, 15, 197
- Poutanen, J., Lipunova, G., Fabrika, S., Butkevich, A. & Abolmasov, P. 2007 *MNRAS*, 377, 1187
- Roberts, T. P. & Colbert, E. J. M. 2003 *MNRAS*, 341, 49
- Rodríguez, M. 2002 *A&A*, 389, 556
- Sánchez, S. F. 2006, *Astronomische Nachrichten*, 327, 850
- Schlegel, D. J. 1994, *ApJL*, 424, 99
- Schlegel, D. J., Finkbeiner, P. F. & Davis, M. 1998, *ApJ*, 500, 525
- Shakura, N. I. & Sunyaev, R. A. 1973, *A&A*, 24, 337
- Shull, J. M. & McKee, C. F. 1979, *ApJ*, 227, 131
- Soria, R., Cropper, M., Pakull, M., Mushotzky, R. & Wu, K. 2005, *MNRAS*, 356, 12
- Soria, R. & Kuncic, Z. 2007, *Advances in Space Research*, 42, 517; arXiv:0705.1374v1
- Swartz, A. D., Ghosh, K. K., Tennant, A. F. & Wu, K., 2004 *ApJS*, 154, 519
- Tully, B. “Nearby Galaxies Catalog” 1998, Cambridge, Cambridge University Press
- Van Dyk, S. D., Sramek, R. A. & Weiler, K. W. 1994, *ApJ*, 425, 77

Table 1. Observational logs

Spectrograph	MPFS	SCORPIO (long-slit mode)
Date	2005/17/01	2005/10/06
Total exposure (s)	5829	5400
Spectral range (\AA)	4000-7000	3900-5700
Spectral resolution (\AA)	6	5
Seeing, arcsec	1.7	1.6

Table 2. MF16 emission line parameters. Line intensities in $H\beta$ units (the uncertainties do not account for the the $H\beta$ flux uncertainty), radial velocities and FWHMs.

line	$\frac{F(\lambda)}{F(H\beta)}$	$\frac{F(\lambda)}{F(H\beta)}$ (unreddened)	$V, km\ s^{-1}$	$FWHM, \text{\AA}$
[SII] λ 4068	0.200 \pm 0.013	0.276 \pm 0.018	-100 \pm 20	8.3 \pm 0.7
$H\delta$	0.228 \pm 0.013	0.311 \pm 0.018	-66 \pm 11	6.6 \pm 0.4
[TiIII] λ 4161?	0.018 \pm 0.008	0.024 \pm 0.010	0 \pm 40	3.8 \pm 1.2
SIII λ 4284?	0.074 \pm 0.012	0.094 \pm 0.015	-50 \pm 40	11.2 \pm 1.3
$H\gamma$	0.408 \pm 0.013	0.510 \pm 0.016	-47 \pm 14	6.2 \pm 0.2
[OIII] λ 4363	0.146 \pm 0.016	0.181 \pm 0.019	-73 \pm 14	7.1 \pm 0.5
[FeII] λ 4414?	0.039 \pm 0.010	0.047 \pm 0.012	-10 \pm 50	8.6 \pm 1.6
HeI λ 4471	0.038 \pm 0.006	0.045 \pm 0.007	-56 \pm 20	6.0 \pm 0.7
[FeIII] λ 4658	0.066 \pm 0.011	0.072 \pm 0.012	10 \pm 30	9.3 \pm 1.2
HeII λ 4686	0.205 \pm 0.009	0.222 \pm 0.010	-5 \pm 18	6.2 \pm 0.2
[FeIII] λ 4701	0.017 \pm 0.008	0.018 \pm 0.008	-35 \pm 50	5.1 \pm 1.7
HeI λ 4713 (+[ArIV] λ 4711?)	0.021 \pm 0.008	0.021 \pm 0.008	-70 \pm 40	5.3 \pm 1.6
[ArIV] λ 4740	0.009 \pm 0.004	0.009 \pm 0.004	-50 \pm 30	3 \pm 1
$H\beta$	1.000 \pm 0.017	1.000 \pm 0.017	-28 \pm 4	6.2 \pm 0.2
[FeIII] λ 4881	0.018 \pm 0.008	0.018 \pm 0.008	-86 \pm 20	4.8 \pm 1.0
HeI λ 4922	0.011 \pm 0.005	0.011 \pm 0.005	-10 \pm 30	3.9 \pm 1.2
[FeIII] λ 4936	0.008 \pm 0.005	0.008 \pm 0.005	-60 \pm 50	4.0 \pm 1.5
[OIII] λ 4959	2.337 \pm 0.050	2.24 \pm 0.05	-23 \pm 3	6.2 \pm 0.1
[FeIII] λ 4986	0.044 \pm 0.010	0.042 \pm 0.009	50 \pm 100	4.0 \pm 1.5
[OIII] λ 5007	6.94 \pm 0.14	6.50 \pm 0.13	-17.4 \pm 2.5	6.2 \pm 0.1
[FeIII] λ 5033?	0.013 \pm 0.005	0.012 \pm 0.005	50 \pm 30	4.1 \pm 1.4
[FeII] λ 5158?	0.073 \pm 0.005	0.064 \pm 0.004	11 \pm 9	7.8 \pm 0.4
[NI] λ 5199	0.152 \pm 0.005	0.131 \pm 0.004	-34 \pm 5	7.1 \pm 2.0
[FeII] λ 5262?	0.072 \pm 0.014	0.061 \pm 0.012	140 \pm 90	18 \pm 2
[FeII] + FeIII λ 5270	0.018 \pm 0.008	0.015 \pm 0.007	60 \pm 30	5.1 \pm 1.7
FeIII λ 5300?	0.011 \pm 0.005	0.009 \pm 0.004	100 \pm 50	5 \pm 2
HeII λ 5411	0.021 \pm 0.005	0.017 \pm 0.004	-10 \pm 20	5.6 \pm 1.0
[NII] λ 5755	0.118 \pm 0.015	0.084 \pm 0.011	-70 \pm 30	16.0 \pm 1.5
HeI λ 5876	0.114 \pm 0.024	0.078 \pm 0.016	-9 \pm 20	7.0 \pm 1.1
[OI] λ 6300	1.421 \pm 0.083	0.89 \pm 0.05	25 \pm 9	10.1 \pm 0.4
[OI] λ 6364	0.480 \pm 0.029	0.296 \pm 0.018	12 \pm 9	9.7 \pm 0.4
[NII] λ 6548	1.385 \pm 0.027	0.822 \pm 0.016	-18.7 \pm 1.3	7.6 \pm 0.1
$H\alpha$	4.728 \pm 0.087	2.80 \pm 0.05	-15.7 \pm 2.1	7.8 \pm 0.1
[NII] λ 6583	4.156 \pm 0.082	2.45 \pm 0.05	-18.6 \pm 2.2	7.6 \pm 0.1
HeI λ 6678	0.060 \pm 0.032	0.035 \pm 0.018	-18 \pm 9	14.0 \pm 5.2
[SII] λ 6717	2.457 \pm 0.024	1.412 \pm 0.014	-37.5 \pm 1.1	7.7 \pm 0.1
[SII] λ 6731	2.348 \pm 0.025	1.346 \pm 0.014	-32.8 \pm 1.2	8.2 \pm 0.1

Table 3. Fitting emission line fluxes with *Cloudy* models. Emission line fluxes are given in 10^{-16} erg cm $^{-2}$ s $^{-1}$.

line	F_{obs}	F_{model}	$\Delta\chi^2$	F_{obs}	F_{model}	$\Delta\chi^2$
$A_V,^m$		1.34			1.54	
Fe III λ 4658	11 \pm 2	30	90	18 \pm 3	35	32
He II λ 4686	44 \pm 2	36	16	56 \pm 2	44	36
H β	200 \pm 3	205	2	249 \pm 4	246	0.56
[O III] λ 5007	1310 \pm 30	1089	54	1620 \pm 30	1520	11
He I λ 5876	16 \pm 3	27	13	20 \pm 4	32	9
[N II] λ 6584	526 \pm 10	484	15	611 \pm 12	527	49
[S II] λ 6717	304 \pm 3	334	100	352 \pm 3	367	25
[S II] λ 6731	290 \pm 3	316	75	335 \pm 4	348	11
F , erg cm $^{-2}$ s $^{-1}$		0.55 $^{+0.1}_{-0.05}$			0.6 $^{+0.1}_{-0.1}$	
T , 10^5 K		5.05 $^{+0.15}_{-0.05}$			5.1 $^{+0.15}_{-0.05}$	
χ^2/DOF		62			25	